Studies on Direct Laser Cladding of SiC Dispersed AISI 316L Stainless Steel

JYOTSNA DUTTA MAJUMDAR and LIN LI

In the present study, attempts have been made to develop SiC dispersed (5 and 20 wt pct) AISI 316L stainless steel matrix composite by direct laser cladding with a high power diode laser. Direct laser cladding has been carried out by melting the powder blends of AISI 316L stainless steel and SiC (5 and 20 wt pct) and, subsequently, depositing it on mild steel (0.15 pct C steel) in a layer by layer fashion to develop a coupon of 100 mm^2 × 10 mm dimension. A continuous, defect-free (microcracks and micro- or macroporosities), and homogeneous microstructure is formed, which consists of a dispersion of partially dissolved SiC (leading to formation of very low fraction of Cr_3C_2 and Fe_2Si) in grain-refined austenite. The microhardness of the clad layer increases from 155 VHN to 250 to 340 VHN (for 5 wt pct SiC dispersed) and 450 to 825 VHN (for 20 wt pct SiC dispersed) as compared to 155 VHN of commercially available AISI 316L stainless steel. The corrosion rate in 3.56 wt pct NaCl solution is significantly reduced in 5 wt pct SiC dispersed steel; however, 20 wt pct SiC dispersed steel showed a similar behavior as the commercially available AISI 316L stainless steel. The processing zone for the development of a defect-free microstructure with improved properties has been established.

© The Minerals, Metals & Materials Society and ASM International 2009

I. INTRODUCTION

AISI 316L stainless steel is used as a structural material in the oil and gas industry, refineries, and chemical and petrochemical plants.[1] However, the wear resistance property of AISI 316L stainless steel is poor.[1] Dispersion of hard ceramic particles in the metallic matrix has received considerable interest due to improvement of strength, stiffness, and wear resistance as compared to their monolithic counterparts.[2] A high power laser beam may be used as a source of heat to melt material in the form of powder/wire and, subsequently, deposit it on a substrate in a layer by layer fashion and build the predetermined shape of the component, known as direct laser cladding.[3] The advantages of laser processing over conventional techniques include a faster processing speed, relative cleanliness, a very high heating/cooling rate (10^5 K/s), high solidification velocity (up to a maximum of 30 m/s), scope of automation and formation of an exotic composition/microstructure, and even metastable and glassy phases. A high power laser beam has been extensively used to disperse ceramic particles on the surface of metallic substrates.[3] Cheng et al.[4] studied the dispersion of ceramic particles (WC, Cr_2C_3, SiC, TiC, CrB, and Cr_2O_3) on austenitic stainless steel UNS S31603 using a laser surfacing technique. Thawari

et al.[5] surface alloyed medium carbon steel with silicon carbide using a high-power CO_2 laser with a considerable improvement in wear resistance. Woldan et al.[6] studied the macrostructure of laser surface alloyed mild steel with SiC. Buytoz and Ulutan[7] coated SiC particles on the surface of austenitic stainless steel using the tungsten inert gas based weld overlaying technique, which led to complete dissolution of SiC with the matrix and formation of dendritric microstructure with precipitation of M_7C_3 primary carbide and improvement in hardness to 550 and 750 HV. Li et al.[8] studied the effect of laser surface clad 30 pct SiC + 70 pct Ni on the microstructure and wear resistance of steel substrate. Dutta Majumdar et al.[9] reported the improvement in wear resistance of AISI 304 stainless steel by laser composite surfacing with SiC. Tassin et al.[10] hardened the surface of AISI 316L stainless steel by preplacing a layer of Cr_3C_2, Cr, Ti, and SiC and subsequently irradiating with a 300 W Nd:YAG laser. The surface alloys were composed of austenite (γ) dendrites surrounded by a γ-M_7C_3 eutectic (M = Fe or Cr); their microhardness ranged from 380 to 450 HV.

Attempts at laser-assisted fabrication of AISI 316L stainless steel have already been made by Pinkerton and Li,[11] who studied the influence of pulse frequency and duration on the microstructure, surface roughness, and hardness of fabricated 316L stainless steel using pulsed wave CO_2 laser. Arcella et al.[12] studied the laser-assisted forming of titanium. Srivastava et al.[13] reported on the direct laser fabrication of Ti48Al2Mn2Nb alloy and established the role of process parameters on the microstructure of the fabricated product. A homogeneous and refined microstructure was achieved, and thermal stability of the microstructure was established. Dutta Majumdar et al.[14,15] studied the effect of laser

JYOTSNA DUTTA MAJUMDAR, Associate Professor, is with the Department of Metallurgy and Materials Engineering, IIT Kharagpur, WB - 721302, India. Contact e-mail: jyotsna@metal.iitkgp.ernet.in LIN LI, Professor, is with the School of Mechanical, Civil and Aerospace Engineering, University of Manchester, Manchester M60 1QD, UK.

parameters on the microstructures and properties of direct laser clad AISI 316L stainless steel and found an enhancement in microhardness and corrosion resistance of the fabricated component. In this regard, it is relevant to mention that, though direct laser cladding has been successfully applied to develop metals/alloys, the technique has not been extensively studied for the development of metal-matrix composites. Recently, Wang et al.[16] reported the development of compositionally graded TiC dispersed Ti-6Al-4V metal matrix composite by direct laser cladding with decreased volume fraction of TiC from the surface toward the core.

In the present study, attempts have been made to develop a silicon carbide dispersed AISI 316L stainless steel metal matrix composite by direct laser cladding. Following fabrication, a detailed characterization of the fabricated layer has been undertaken and properties such as hardness and corrosion resistance have been studied in detail. Following a detailed correlation between the microstructures, phases, microhardness, corrosion resistance of the fabricated parts, and laser parameters, the optimum processing zone for the development of a defect-free microstructure with improved properties has been established.

II. EXPERIMENTAL PROCEDURE

In the present study, gas-atomized powder blends of AISI 316L stainless steel (particle size of 45 to 60 μm) and SiC (particle size of 25 to 40 μm) in the weight ratio of 95:5 and 80:20 were used as feedstock material. A Laserline diode laser with mixed 810- and 940-nm wavelengths, at a ratio of 1:1 (maximum power of 1.5 kW) and with optical fiber beam delivery system (with a spot size of 3.5×2 mm^2), was used for processing. Fabrication of the layer was conducted by melting the feedstock powder (delivered by an external powder feeder) using laser deposition of the melt on the mild steel in a layer by layer fashion to build a coupon of dimensions 20 mm $\times$ 20 mm $\times$ 10 mm. The entire process was carried out using Ar as the shrouding environment (at a flow rate of 6 L/min) to avoid oxidation during lasing. The substrate was mounted on a CNC controlled X-Y sweeping stage, and a relative speed between the laser beam and substrate was maintained to ensure the area coverage and a finite time of interaction between the laser beam and powder. Figure 1 shows the schematic of the direct laser cladding technique used in the present study. The main process variables for the present study were applied power (700 to 1100 W), scan speed (3.5 to 7.5 mm/s), and powder feed rate (60 mg/s) at an argon flow rate of 5 L/min. Table I summarizes the detailed process parameters used for direct laser cladding. Following fabrication, a detailed microstructural study of the top surface and cross section of the fabricated component was conducted by optical microscopy. The microstructure of each layer at different locations and the interface between two layers were carefully observed at a higher magnification using scanning electron microscopy. Composition analysis of the fabricated layer was carried out using energy-dispersive
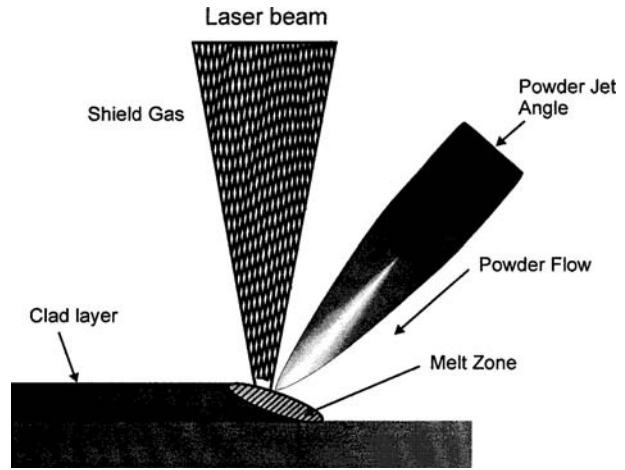

Fig. 1—Schematic of the direct laser cladding technique.

Table I. Summary of Laser Parameters Employed for Direct Laser Cladding

Solution	Composition	Applied Power (W)	Scan Speed (mm/s)
1	5 wt pct SiC dispersed AISI 316L stainless steel	700	3.5 to 7.5
2	do	800	3.5 to 7.5
3	do	900	3.5 to 7.5
4	do	1000	4.5 to 7.3
5	20 wt pct SiC dispersed AISI 316L stainless steel	700	3.5 to 7.5
6	do	800	3.5 to 7.5
7	do	900	3.5 to 7.5
8	do	1000	3.5 to 7.5

spectroscopic (EDS) analysis using ZAF correction. Phases present in the build-up layer were analyzed by the X-ray diffraction technique using a PHILIPS* X-ray

---

*PHILIPS is a trademark of FEI Company, Hillsboro, OR.

---

diffractometer and Cu as target material (wavelength = 1.5405 A). The microhardness of the fabricated layer was measured using a Vicker's microhardness tester with an applied load of 100 g and correlated with process parameters.

Finally, the pitting corrosion behavior of direct laser clad SiC dispersed AISI 316L stainless steel was compared with that of the as-received stainless steel by calculating the corrosion rate derived from the potentiodynamic anodic polarization study in a 3.56 wt pct NaCl using standard calomel electrode as the reference electrode and platinum as the counter electrode.[17] Polarization was carried out from −500 to +5000 mV(SCE) at a scan rate of 2 mV/s. A Tafel plot[17] was constituted from the logarithm of the current density value as a function of voltage. The slope of the Tafel plot in the linear region in the anodic direction is referred to as the

anodic Tafel constant and that in the cathodic direction is called the cathodic Tafel constant. Corrosion current (i_{corr}) was determined from the intersection of these two linear plots. Subsequently, the pitting corrosion behavior was determined by measuring the primary potential for pit formation, E_{pp1} (the potential at which there is a sudden rise in current density with a small increase in potential).

III. RESULTS AND DISCUSSION

In the present section, a detailed characterization of the fabricated parts and its properties are presented.

A. Characteristics of the Clad Layer

In the present study, a detailed observation of the optical, scanning, and transmission electron micrographs of the top surface and cross section of direct laser clad layers was undertaken to study the morphology, grain size, and defect density of the fabricated components, and the effect of laser parameters on them. Figure 2 shows the scanning electron micrograph of the top surface of SiC dispersed (5 wt pct) AISI 316L stainless steel lased with a power of 700 W and scan speed of 7.5 mm/s. The microstructure consists of dispersion of SiC in grain-refined AISI 316L stainless steel matrix. The interface between SiC particles and the matrix is defect free; *i.e.*, it is free from any porosity or microcrack. From Figure 2, it is also evident that there is a marginal dissolution of SiC particle from the interface. The dissolution is evident from the irregular shape of the particle (from its initial globular shape) and marginal decrease in particle size. The microstructure of the matrix is predominantly dendritic in nature with an average interdendritic secondary arm spacing ranging from 3 to 10 μm for different conditions of lasing. Increase in applied power and decrease in scan speed are found to coarsen the microstructure. Figures 3(a) and (b) show the scanning electron micrographs of the top surface of direct laser clad AISI 316L stainless steel dispersed with 20 wt pct SiC lased with a scan speed of 7.5 mm/s and at a power of (a) 700 W and (b) 900 W. From Figure 3, it is clear that the microstructure consists of a very high volume fraction of fine precipitates containing silicon carbide and iron silicides
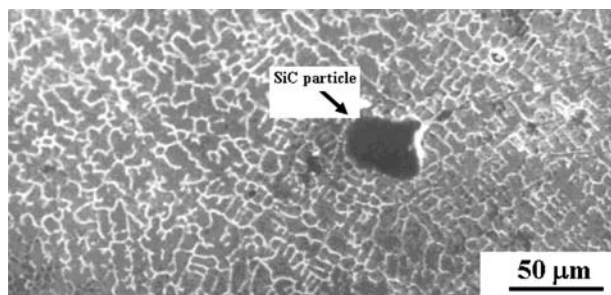
Fig. 2—Scanning electron micrograph of the 5 wt pct SiC dispersed AISI 316 stainless steel lased with a power of 700 W and scan speed of 7.5 mm/s.

(as evident by X-ray diffraction analysis). Furthermore, there is a coarsening of microstructure and decrease in volume fraction of SiC particles (predominantly due to dissolution of SiC) with an increase in applied power. A detailed EDS spot analysis at the grain and along the grain boundary regions of Figure 3(a) are summarized in Table II. From the elemental distribution in grain and along the grain boundary region, it may be noted that the grain boundary regions are enriched in Cr and Si. Hence, the bright network interconnecting the grain boundary is due to the presence of very fine silicon carbide (SiC), chromium carbide (Cr_3C_2), and iron silicide (Fe_2Si), which is also confirmed by X-ray diffraction analysis. In this regard, it is relevant to note that dissolution of SiC into Si and C occurs at 1200 °C and forms iron silicides having different stoichiometry when it is in contact with molten iron.[18,19] Hence, it may be concluded that the grain boundary precipitates
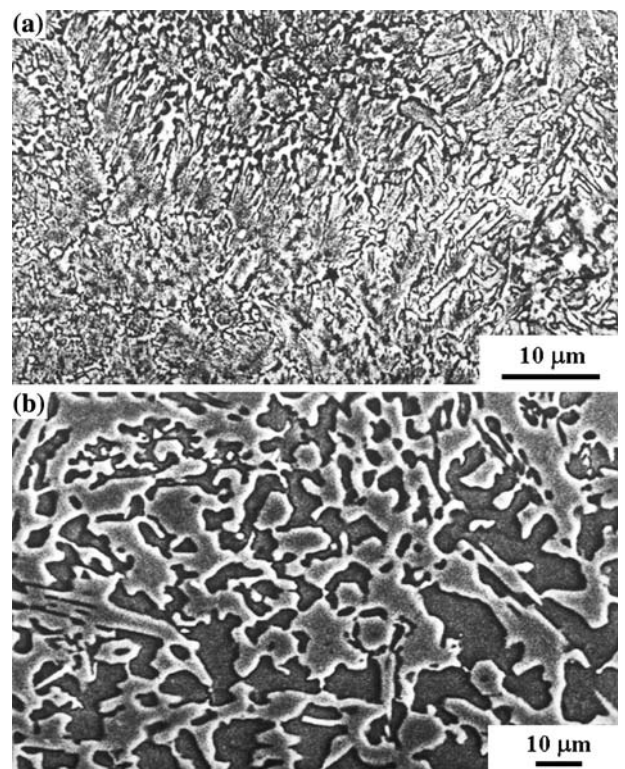
Fig. 3—Scanning electron micrographs of the top surface of direct laser clad AISI 316L stainless steel dispersed with 20 wt pct SiC lased with a power of (*a*) 700 W and (*b*) 900 W and scan speed of 7.5 mm/s.

Table II. Composition Distribution along the Grain and Grain Boundary Regions in Figure 3(a)

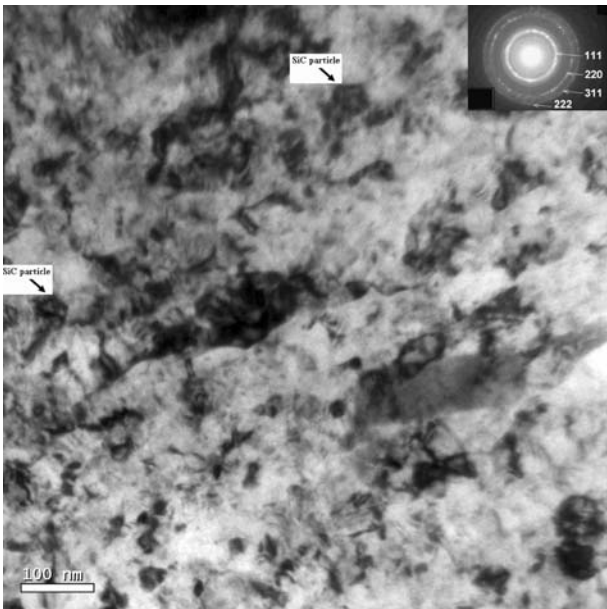| Position | Composition (Wt Pct), Percentage Error: 0.1 Pct | | | | |
	Si	Cr	Fe	Ni	Mo
Grain	nil	18	70	8	4
Grain boundary	10	22	56	8	4

Fig. 4—High-resolution transmission electron micrograph of the direct laser clad AISI 316L stainless steel dispersed with 20 wt pct SiC lased with a power of 700 W and scan speed of 7.5 mm/s.

are predominantly of iron silicide, silicon carbides, and chromium carbide. Figure 4 shows the high-resolution transmission electron micrograph of 20 wt pct SiC dispersed AISI 316L stainless steel lased with a power of 700 W and scan speed of 7.5 mm/s. From Figure 4, it may be noted that the microstructure consists of nanograined silicon carbide; the corresponding SAD pattern is embedded in the micrograph. A significant refinement of SiC particle size following laser processing is possibly by a dissolution and reprecipitation process due to a very large cooling rate achieved during laser processing.

Apart from grain morphology, grain size plays a crucial role in determining the properties of a component. Laser power and scan speed both play roles in determining the final grain size of the developed parts. In the present study, a detailed investigation of the influence of laser parameters on the grain size/interdendritic secondary arm spacing is undertaken. Figures 5(a) and (b) show the variation of average grain size or secondary dendrite arm spacing of the fabricated coupon with scan speed at an applied power of 800, 900, and 1000 W in (a) 5 wt pct SiC and (b) 20 wt pct SiC dispersed AISI 316L stainless steel. From Figure 5(a), it may be noted that grain size decreases with increase in scan speed. Refinement of microstructure with increase in scan speed is mainly due to a rapid quenching rate. A similar trend was also noticed in direct laser clad AISI 316L stainless steel with 20 wt pct SiC dispersion (*cf*. Figure 5(b)). However, a comparison between Figures 5(a) and (b) shows that a finer grain size was obtained for 20 wt pct SiC dispersed AISI 316L stainless steel as compared to 5 wt pct SiC dispersed AISI 316L stainless steel when lased under the same parameters. On the other hand, increasing applied power
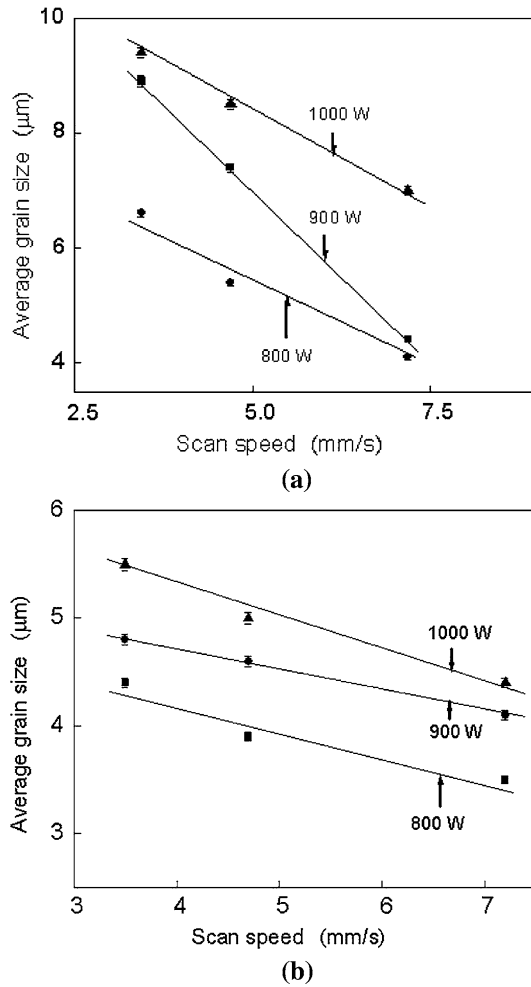

Fig. 5—Variation of average grain size in direct laser clad (*a*) 5 wt pct and (*b*) 20 wt pct SiC dispersed AISI 316L stainless steel with scan speed at an applied power of 800 W (plot 1), 900 W (plot 2), and 1000 W (plot 3).

increases the grain size of the fabricated coupons in direct laser clad SiC dispersed AISI 316L stainless steel (in both 5 and 20 wt pct dispersions). Increased grain size of the fabricated coupon with increase in applied power is due to a decreased rate of cooling when applying a higher power during melting of powder. Apart from microstructure, microstructural homogeneity plays an important role in producing uniform mechanical and electrochemical properties of the fabricated layer. In direct laser clad layer, variation of grain size at different positions of the fabricated layer is a commonly encountered problem. The average grain size, though, shows an average trend; grain size was highly refined at the near surface region but coarser at the interface between two successive layers. The variation of grain size in the same sample is attributed to (a) the differential rate of cooling at different zones (*i.e.*, a maximum cooling rate at the surface and minimum at the intermediate region), (b) the heat extraction from the newly developed layer to the underlying substrate (annealing of the first layer due to the heat extraction from the second layer), and (c) the annealing of the

overlapped zone due to overlapping. The range of grain size (difference between the maximum and minimum grain size) was chosen as a measure of the degree of homogeneity in the microstructure; the lower the grain size range, the more homogeneous is the microstructure. The range of grain size was found to vary with the combined influence of applied power and scan speed. Figures 6(a) and (b) summarize the effect of laser power and scan speed combinations on the grain size range of direct laser clad SiC dispersed AISI 316L stainless steel with (a) 5 wt pct and (b) 20 wt pct SiC dispersion. From Figure 6(a), it is clear that in direct laser clad AISI 316L stainless steel with 5 wt pct SiC, the range of grain size varies with a close range of 4 to 5 μm except for a few combinations of applied power and scan speed. However, no specific trend was observed to conclude the individual influence of applied power and scan speed on the range of grain size (cf. Figure 6(a)). Figure 6(b) represents the variation of range of grain size at different combinations of applied power and scan speed for direct laser clad SiC (20 wt pct) dispersed AISI 316L stainless steel. From Figure 6(b), it is clear that the range of grain

size varied within a very close range of 6 to 7 μm, though a minimum size range (2 to 4 μm) was observed at the combination of a high power and a high scan speed. An increased average grain size range in 20 wt pct SiC dispersed steel (6 to 7 μm) as compared to the 5 wt pct SiC dispersed one (4 to 5 μm) is attributed to the presence of a large quantity of dispersions (silicon carbide, chromium carbide, and iron silicide) in the former leading to a large fluctuation in thermal history with position as compared to the latter.

Figure 7 shows the X-ray diffraction profiles of commercially available AISI 316L stainless steel (curve a) and direct laser clad 5 wt pct SiC dispersed (curve b) and 20 wt pct SiC dispersed (curve c) AISI 316 stainless steel with power of 700 W and scan speed of 7.5 mm/s. A close comparison between curves a and b in Figure 7 shows that there is a presence of SiC and only a few Cr_3C_2 along with γ-stainless steel in direct laser clad 5 wt pct SiC dispersed AISI 316L stainless steel. However, the presence of a few Fe_2Si peaks was also observed in the X-ray diffraction profile of direct laser clad 20 wt pct SiC dispersed AISI 316L stainless steel (curve c). From the X-ray diffraction profiles, it may be concluded that SiC particles were partially dissociated and there was formation of a measurable quantity of Cr_3C_2 and Fe_2Si phase in the microstructure. In this regard, it is relevant to mention that the formation of different silicides of iron, mainly Fe_2Si, Fe_3Si, and FeSi, based on the Si content in the system, has been reported in the literature.[4,20] Laser surface alloying and cladding of stainless steel SiC composite have also revealed the formation of Cr_7C_3 phases.[21] Thawari et al.[5] reported the formation of $C_{0.12}Fe_{0.79}Si_{0.09}$, Fe_2Si, Fe_3Si, Fe_7C_3, and Fe_3C phases while laser surface alloying of SiC on medium carbon steel. However, laser processing under the present set of parameters could avoid complete dissolution of SiC particles, as was observed by other studies while laser surface alloying or cladding with SiC.[4,5,20,21]
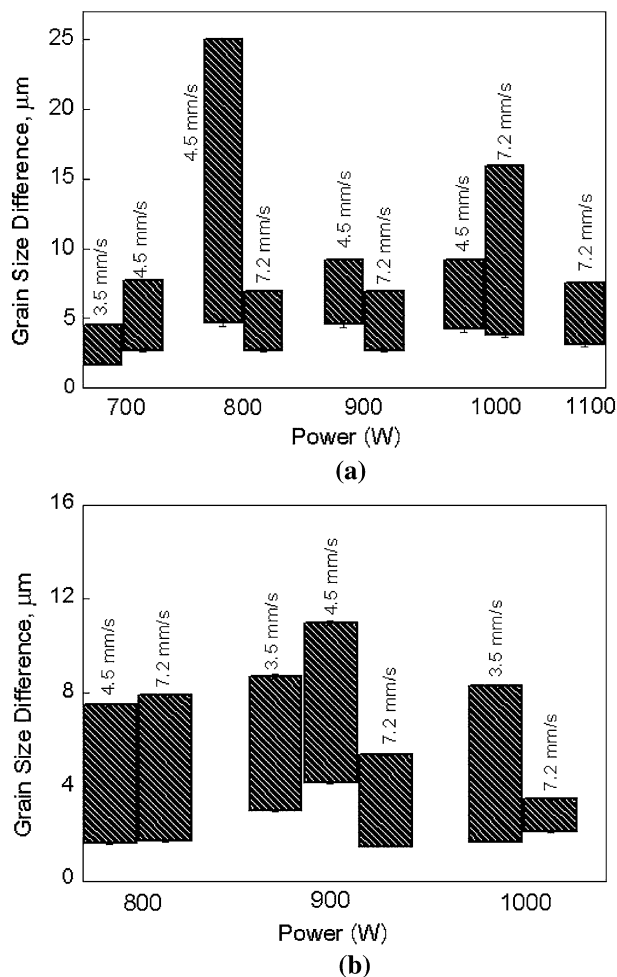

(a)

(b)

Fig. 6—Bar chart showing the range of grain size at different combinations of applied power and scan speed in direct laser clad (a) 5 wt pct SiC and (b) 20 wt pct SiC dispersed 316L stainless steel.
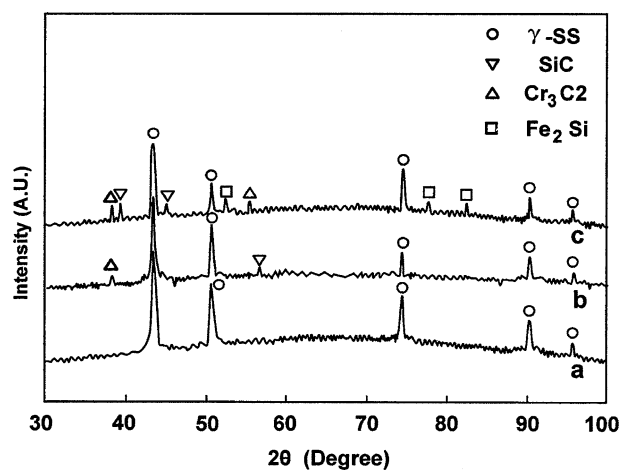

Fig. 7—X-ray diffraction profiles of commercially available AISI 316L stainless steel (plot a) and direct laser clad SiC dispersed, 5 wt pct (plot b) and 20 wt pct (plot c) AISI 316L stainless steel lased with a power of 700 W and scan speed of 7.5 mm/s.

B. Properties of the Clad Layer

Figures 8(a) and (b) show the variation of average microhardness in the clad zone of direct laser clad (a) 5 wt pct and (b) 20 wt pct SiC dispersed AISI 316L stainless steel with scan speed at an applied power of 800, 900, and 1000 W. The average microhardness of the clad layer increases to as high as 340 VHN as compared

to 155 VHN of commercially available AISI 316L stainless steel in 5 wt pct SiC dispersed AISI 316L stainless steel. From Figure 8(a), it is observed that the microhardness of the clad layer increases with an increase in scan speed, which is attributed to grain refinement and a lesser extent of SiC dissolution. From Figure 8(b), it may be noted that the microhardness of the direct laser clad 20 wt pct SiC dispersed AISI 316 stainless steel varies between 300 and 800 VHN depending on the laser parameters. A close comparison between Figures 8(a) and (b) shows that the hardness achieved in 20 wt pct SiC dispersed AISI 316L stainless steel was significantly higher than 5 wt pct SiC dispersed AISI 316L stainless steel. The improved microhardness in 20 wt pct SiC dispersed AISI 316L stainless steel is attributed to the presence of an increased volume fraction of SiC and an increased extent of dissociated SiC. Increased hardness of the clad layer with scan speed is predominantly due to grain refinement. From Figure 8, it is also evident that the average microhardness of the clad layer decreases with an increase in applied power. The decrease in microhardness with the increase in applied power is possibly due to grain coarsening at an increased power. The increasing microhardness of the clad coupons is attributed to dispersion of SiC and precipitations of Cr_2C_3 and Fe_2Si in the microstructure.

The electrochemical behavior of the SiC dispersed AISI 316L stainless steel fabricated coupon was evaluated in a 3.56 wt pct NaCl solution and compared with as-received AISI 316L stainless steel. Table III summarizes the electrochemical parameters of as-received and direct laser clad 5 wt pct SiC dispersed AISI 316L stainless steel lased for different conditions of lasing derived from polarization study in Hank's solution. From the corrosion rate, the general corrosion behavior of the component may be predicted. From Table III, it is seen that the corrosion rate is significantly reduced in 5 wt pct SiC dispersed AISI 316L stainless steel as compared to conventionally available AISI 316L stainless steel in almost all processing conditions. Furthermore, the corrosion rate increases with an increase in scan speed. Increasing the scan speed causes refinement of the microstructure and a high volume fraction of SiC, increasing the numbers of anodic sites and interface as a result the corrosion rate increases. The presence of dissociated Si may cause an improvement in corrosion resistance. On the other hand, in direct laser clad 20 wt pct SiC dispersed stainless steel, the corrosion rate is almost equivalent to the as-received AISI 316L
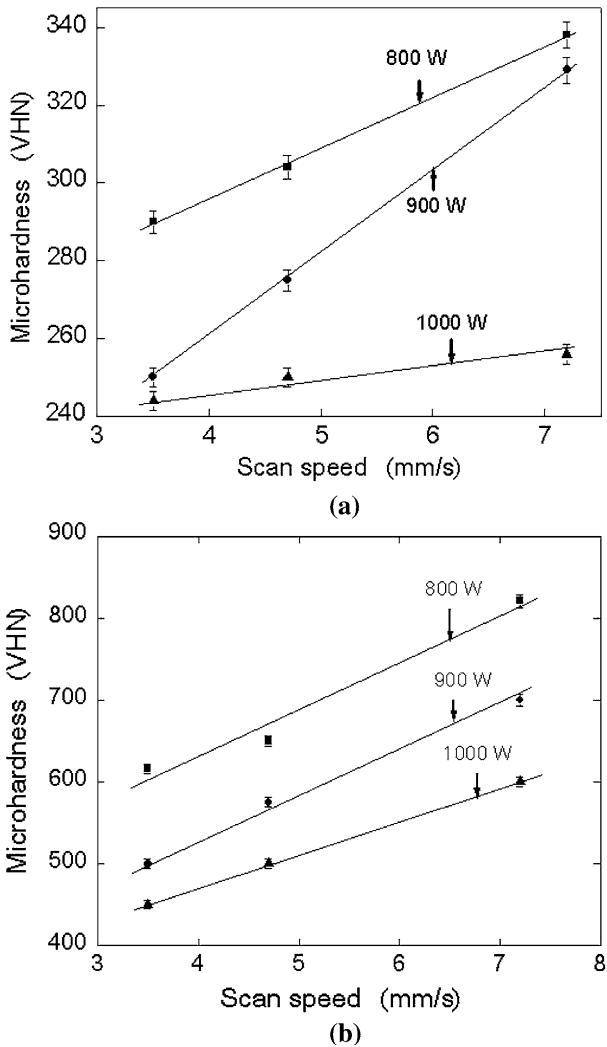

Fig. 8—Variation of average microhardness of the clad zone in direct laser clad (a) 5 wt pct and (b) 20 wt pct SiC dispersed AISI 316L stainless steel with scan speed, at an applied power of (1) 800 W, (2) 900 W, and (3) 1000 W.

Table III. Summary of Corrosion Behaviors of SiC Dispersed AISI 316L Stainless Steel

Sample Details	Applied Power (W)	Scan Speed (mm/s)	Corrosion Rate (mm/year)
AISI 316L stainless steel	—	—	2.5×10^{-2}
5 wt pct SiC dispersed AISI 316L stainless steel	700 to 1000	3.5	0.15×10^{-2} to 1.2×10^{-2}
		4.5	0.15×10^{-2} to 2.1×10^{-2}
		7.5	1.0×10^{-2} to 2.75×10^{-2}
20 wt pct SiC dispersed AISI 316L stainless steel	700 to 1000	3.5	2.5×10^{-2}
		7.5	2.6×10^{-2}

stainless steel and was not found to vary significantly with laser parameters.

IV. PROCESS OPTIMIZATION

From the present investigations, it is revealed that process parameters (laser power and scan speed) play an important role in determining the characteristics (microstructures, phases, and composition) and properties (mechanical and electrochemical) of the direct laser clad zone. Figure 9 shows the processing regime for direct laser cladding of SiC (5 and 20 wt pct) dispersed AISI 316L stainless steel, which shows the combinations of laser power and scan speed for the formation of a defect-free and homogeneous microstructure. If the applied power is too low or scan speed is too high, it causes inadequate melting. On the other hand, at a very high applied power or too low a scan speed, there is evaporation and crater formation. However, the microstructures and properties of the fabricated coupons showed a wide variation depending on the choice of applied power and scan speed combinations. From the average trend of the variation of microstructures and properties with laser parameters, the overall processing regime for direct laser clad SiC dispersed AISI 316L stainless steel was divided into two zones, as shown in Figure 9. The corresponding properties of the clad layer are summarized in Table IV. From Table IV, it may be
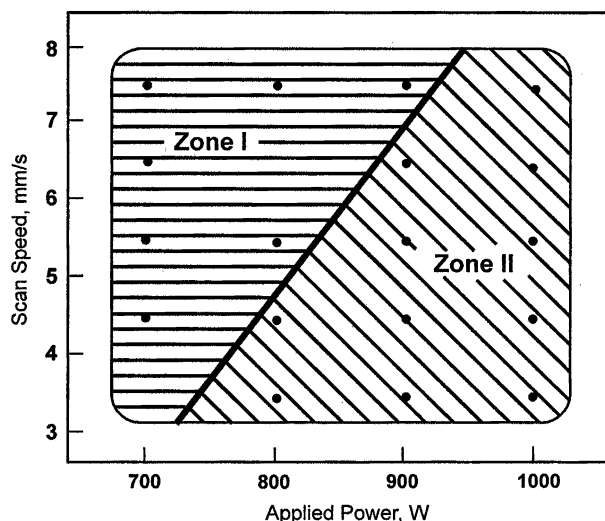
noted that, in 5 wt pct SiC dispersed AISI 316L stainless steel, at a combination of low power and high scan speed (zone I), there will be microstructural refinement, increased hardness, and an improved corrosion resistance (as compared to commercially available AISI 316L stainless steel). On the other hand, a combination of high power and low scan speed leads to coarsening of microstructure, decreased hardness, and a higher corrosion resistance. However, corrosion resistance was always higher or equivalent to as-received AISI 316L stainless steel in this case. In the case of 20 wt pct SiC dispersed AISI 316L stainless steel, though, grain size and microhardness followed a similar trend (with process parameters) as compared to 5 wt pct SiC dispersed AISI 316L stainless steel; however, corrosion resistance in the direct laser clad sample was almost similar to the conventionally available AISI 316L stainless steel and was not influenced much with laser parameters. In this regard, it is relevant to mention that a maximum improvement in mechanical properties is achieved when lased at an applied power of 700 W and a scan speed of 7.5 mm/min for both 5 and 20 wt pct SiC dispersed AISI 316L stainless steel.

V. SUMMARY AND CONCLUSIONS

In the present study, the detailed study on direct laser clad SiC (5 and 20 wt pct) dispersed AISI 316L stainless steel has been carried out with a power of 700 to 1100 W, scan speed of 3 to 8 mm/s, and powder feed rate of 60 mg/s (at an argon flow rate of 5 L/min). From the present study, the following conclusions may be drawn.

1. A continuous, defect-free, and homogeneous microstructure is formed, which consists of partially dissociated SiC, Cr_3C_2, and Fe_2Si (only in 20 wt pct SiC dispersoids) in grain-refined austenite. Grain size increases with increase in applied power and decrease in scan speed.
2. Average microhardness of the clad layer decreases with increase in applied power and increases with increase in scan speed. The microhardness of the clad layer increases as high as 250 to 340 VHN (for 5 wt pct SiC) and 450 to 800 VHN (for 20 wt pct SiC dispersed) as compared to 155 VHN of commercially available AISI 316L stainless steel. The improved hardness is attributed to dispersion of SiC and precipitations of Cr_2C_3 (in both 5 and 20 wt pct SiC dispersion) and Fe_2Si (in only 20 wt pct SiC dispersion) in the microstructure.

Fig. 9—Processing zone for direct laser cladding of SiC dispersed (5 and 20 wt pct) AISI 316L stainless steel.

Table IV. Properties in Different Regions of Figure 9

Sample		Grain Size	Microhardness	Corrosion Rate (mm/year)
5 wt pct SiC dispersed AISI 316L stainless steel	zone I	4 to 5.5	300 to 340	1.0 to 2.75×10^{-2}
	zone II	6 to 9.5	245 to 290	0.15 to 1.0×10^{-2}
20 wt pct SiC dispersed AISI 316L stainless steel	zone I	3.5 to 4.1	650 to 825	2.6×10^{-2}
	zone II	4.5 to 5.5	450 to 600	2.5×10^{-2}

3. The corrosion rate in Hank's solution is significantly reduced in 5 wt pct SiC dispersed AISI 316L stainless steel. However, in 20 wt pct SiC dispersed AISI 316L, a similar corrosion behavior is observed as in commercially available AISI 316L stainless steel.
4. The optimum process parameters corresponding to a maximum improvement in hardness (for both 5 and 20 wt pct SiC dispersed AISI 316L stainless steel) were the following: applied power of 700 W and scan speed of 7.5 mm/min.

ACKNOWLEDGMENTS

REFERENCES

1. C.J. Novak: in *Handbook of Stainless Steels*, D. Peckner and I.M. Bernstein, eds., McGraw-Hill, New York, NY, 1977, p. 1.
2. *An Introduction to Metal Matrix Composites*, T.W. Clyne and P.J. Withers, eds., Cambridge University Press, Cambridge, United Kingdom, 1993.
3. *Laser Material Processing*, W.M. Steen, ed., Springer Verlag, New York, NY, 1991, p. 1.
4. F.T. Cheng, C.T. Kwok, and H.C. Man: *Surf. Coat. Technol.*, 2001, vol. 139, pp. 14–24.
5. G. Thawari, G. Sundararajan, and S.V. Joshi: *Thin Solid Films*, 2003, vol. 423, pp. 41–53.
6. A. Woldan, J. Kusiński, and E. Tasak: *Mater. Chem. Phys.*, 2003, vol. 81, pp. 507–509.
7. S. Buytoz and M. Ulutan: *Surf. Coat. Technol.*, 2006, vol. 200, pp. 3698–3734.
8. Q. Li, G.M. Song, Y.Z. Zhang, T.C. Lei, and W.Z. Chen: *Wear*, 2003, vol. 254, pp. 222–29.
9. J. Dutta Majumdar, B. Ramesh Chandra, A.K. Nath, and I. Manna: *Phys. Status Solidi (a)*, 2006, vol. 203, pp. 2260–65.
10. C. Tassin, F. Laroudie, M. Pons, and L. Lelait: *Surf. Coat. Technol.*, 1996, vol. 80, pp. 207–10.
11. A.J. Pinkerton and L. Li: *Appl. Surf. Sci.*, 2003, vol. 208, pp. 405–10.
12. F.G. Arcella and F.H. Froes: *J. Met.*, 2000, vol. 52, pp. 28–30.
13. D. Srivastava, I.T.H. Chang, and M.H. Loretto: *Intermetallics*, 2001, vol. 9, pp. 1003–13.
14. J. Dutta Majumdar, A. Pinkerton, Z. Liu, I. Manna, and L. Li: *Appl. Surf. Sci.*, 2005, vol. 247, pp. 320–27.
15. J. Dutta Majumdar, A. Pinkerton, Z. Liu, I. Manna, and L. Li: *Appl. Surf. Sci.*, 2005, vol. 247, pp. 373–77.
16. F. Wang, J. Mei, H. Jiang, and X. Wu: *Mater. Sci. Eng.*, 2007, vols. A445–A446, pp. 461–66.
17. "Standard Recommended Practice for Conducting Cyclic Potentiodynamic Polarization Measurements for Localized Corrosion," *Annual Book of ASTM Standards*, ASTM, Philadelphia, PA, 1985, p. G61.
18. S. Kalogeropoulou, L. Baud, and N. Eustathopoulos: *Acta Metall. Mater.*, 1995, vol. 43, pp. 907–12.
19. T. Iseki: in *Silicon Carbide—I*, Somiya and Y. Inomata, eds., Elsevier Science, New York, NY, 1991, p. 247.
20. J. Lacaze and B. Sundman: *Metall. Trans. A*, 1991, vol. 22A, pp. 2211–23.
21. G. Abbas and U. Ghazanfar: *Wear*, 2005, vol. 258, pp. 258–64.